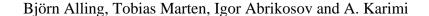# Linköping University Post Print

Comparison of thermodynamic properties of cubic Cr$_{1-x}$ Al$_x$ N and Ti$_{1-x}$ Al$_x$ N from first-principles calculations

Björn Alling, Tobias Marten, Igor Abrikosov and A. Karimi

N.B.: When citing this work, cite the original article.

Comparison of thermodynamic properties of cubic $Cr_{1-x}Al_xN$ and $Ti_{1-x}Al_xN$ from first-principles calculations

B. Alling[a)]
Institute of Physics of Complex Matter, Swiss Federal Institute of Technology Lausanne (EPFL), 1015 Lausanne, Switzerland and Department of Physics, Chemistry and Biology (IFM), Linköping University, SE-581 83 Linköping, Sweden

T. Marten and I. A. Abrikosov
Department of Physics, Chemistry and Biology (IFM), Linköping University, SE-581 83 Linköping, Sweden

A. Karimi
Institute of Physics of Complex Matter, Swiss Federal Institute of Technology Lausanne (EPFL), 1015 Lausanne, Switzerland

In order to investigate the stability of the cubic phase of $Cr_{1-x}Al_xN$ at high AlN content, first principles calculations of magnetic properties, lattice parameters, electronic structure, and mixing enthalpies of the system were performed. The mixing enthalpy was calculated on a fine concentration mesh to make possible the accurate determination of its second concentration derivative. The results are compared to calculations performed for the related compound $Ti_{1-x}Al_xN$ and with experiments. The mixing enthalpy is discussed in the context of isostructural spinodal decomposition. It is shown that the magnetism is the key to understand the difference between the Cr- and Ti-containing systems. $Cr_{1-x}Al_xN$ turns out to be more stable against spinodal decomposition than $Ti_{1-x}Al_xN$, especially for AlN-rich samples which are of interest in cutting tools applications. © *2007 American Institute of Physics*. [DOI: 10.1063/1.2773625]

I. INTRODUCTION

The coating of drills and cutting tools by transition metal nitrides has been used in industrial applications for many decades. TiN, which dominated originally, has gradually been replaced by more sophisticated multicomponent nitrides. Alloying of TiN with Al improves the cutting performance of the coatings. This has been attributed to the increase in oxidation resistance of the Al containing coating. Recently an age hardening mechanism, arising from spinodal decomposition of $B1$ structure $Ti_{1-x}Al_xN$ into coherent cubic domains of AlN and Ti-enriched $Ti_{1-x}Al_xN$ has been suggested[1] as another reason for the improved properties. The experimental observation of isostructural decomposition were later confirmed by the results of first-principles calculations.[2] It was also shown that the driving force of this decomposition is mainly due to an electronic band structure effect in Al-rich samples. However, the same spinodal mechanism that leads to age hardening might be the first step in a process that leads to a nucleation of hexagonal AlN already during growth. This is detrimental for cutting performance[3] and, hence, limits the Al content of the $Ti_{1-x}Al_xN$ coatings.

A related material, $Cr_{1-x}Al_xN$, has also attracted a substantial interest and is in commercial use. Comparing $Cr_{1-x}Al_xN$ with $Ti_{1-x}Al_xN$, the Cr-containing system shows slightly lower hardness for the same Al content. However, a larger amount of Al can be solved in the $B1$ phase without the formation of hexagonal AlN and the stability of $Cr_{1-x}Al_xN$ coatings can be preserved up to higher temperatures.[3–7] There is no experimental report of spinodal decomposition in $Cr_{1-x}Al_xN$. The single phase $B1$ structure can be obtained for AlN content x higher than $x=0.70$,[8] which is impossible for $Ti_{1-x}Al_xN$. Thus, the choice of coating depends on the conditions and cutting requirements of each specific application.

One fundamental difference between the two systems is that the Cr-containing system is magnetic. The ground state of stoichiometric CrN is an orthorhombic structure with a double-layer antiferromagnetic configuration with one of the angles of the underlying $B1$ lattice, $\alpha=88.23°$,[9] being slightly smaller than the ideal value 90°. The Néel temperature has been reported to be around room temperature.[9,10] Above this temperature the material form the cubic $B1$ structure. However, it has been shown that the cubic phase could be stabilized at even lower temperatures, at least down to 20 K, in samples prepared by epitaxial growth.[11,12] In those experiments no magnetic phase transition could be detected. Moreover, the experiment presented in Ref. 11, $B1$ CrN was shown to exhibit a Mott-type insulator behavior at very low temperatures. This effect cannot bee captured by standard first-principles density functional calculations.[13] However, at room temperature, where a disordered magnetic state decreases the splitting of spin up and down states and smears out magnetically induced fine structure, the system shows finite density of states at the Fermi level.[12] The effect is clearly larger than what could be expected from pure Fermi–Dirac smearing at 300 K. We will show that our model for the disordered magnetic state gives results in very good agreement with the corresponding experimental study.

a)Electronic mail: bjoal@ifm.liu.se

102, 044314-1

Although a substantial amount of experimental results has been published considering $Cr_{1-x}Al_xN$ for hard coatings applications and pure CrN has been the subject of first-principles calculations,[13] we are not aware of any first-principles theoretical study of magnetic and thermodynamical properties of $B1$ $Cr_{1-x}Al_xN$ alloys. Previous theoretical works used different approaches to understand the physics of Al containing ternary nitrides and focused on the crossing point of the binding energy curves of the cubic and hexagonal structures of the alloys.[14,15] However, the possibility of isostructural decomposition is as important for the understanding of the physics of hard coating nitrides as the decomposition which involves structural modifications.[1,2]

In this work we present the result of first-principles calculations of the magnetic properties, electronic structure, lattice parameter, and mixing enthalpy of $B1$ $Cr_{1-x}Al_xN$. We compare the results with the recent calculations of $Ti_{1-x}Al_xN$,[2] as well as with the available experimental data. The mixing enthalpy is calculated on a fine concentration mesh so that its second concentration derivative can be derived. The second concentration derivative of the free energy is the key property which needs to be calculated in order to understand whether the system has a tendency toward spontaneous spinodal decomposition or if a nucleation and growth process is necessary for decomposition in a nonequilibrium system. The mixing enthalpy and its second concentration derivative are the starting point for making such a thermodynamic analysis.

II. CALCULATIONAL DETAILS

We have performed first-principles density functional theory (DFT) calculations using a Green's function technique[16–18] within the Koringa–Kohn–Rostocker[19,20] framework and the atomic sphere approximation.[21,22] The substitutional disorder between Cr and Al atoms were treated analytically using the coherent potential approximation (CPA).[23–25] The magnetically disordered phase was modeled using the disordered local moments (DLM) approximation.[26] In this approach, the CPA is used to model a system with finite magnetic moments that have their directions in spin-space randomly distributed between up and down with equal probability. Technically this is done by representing a $(Cr_{1-x}Al_x)N$ alloy with a $(Cr^{\uparrow}_{(1-x)/2}Cr^{\downarrow}_{(1-x)/2}Al_x)N$ system.

The generalized gradient approximation[27] (GGA) was used for the exchange-correlation functional. Local relaxations in the lattice, the atomic shifts away from the ideal $B1$ lattice points due to different chemical environment of different atoms, were considered using the independent sublattice model (ISM) described in details in Ref. 2. The projector augmented wave (PAW) method, as implemented in the Vienna *ab initio* simulation package (VASP),[28–30] was used to calculate the relaxation parameters used in the ISM scheme, as well as to estimate the energy difference between the $B1$ and hexagonal phase of AlN. The lattice parameter for the latter was also determined from the PAW calculations. The total energy was converged to an accuracy of 0.5 meV/atom with respect to the number of k points used for the integration over the Brillouin zone. The nitrogen sublattice was con-

sidered to be completely occupied. The study of nitrogen vacancies is the topic of a future project. The mixing enthalpy was calculated with concentration steps of 5% giving a total of 21 enthalpy points. In order to avoid numerical noise in the calculations of the concentration derivatives, a fifth order polynomial fit to the enthalpy points was used, followed by the analytical calculation of the derivative. All calculations were performed for the cubic $B1$ structure. This is motivated by the experimental fact that the system crystallizes in this structure at least for compositions between $x = 0.00$ and $x = 0.71$ when epitaxially grown under physical vapor deposition conditions. It remains within this structure up to temperatures around 950 °C.[8] If there exists a decomposition within this range of temperatures and concentrations, it should be isostructural, similar to what has been observed for other cubic transition metal nitrides.[1,3]

III. RESULTS

A. Magnetic structure of $Cr_{1-x}Al_xN$

The magnetic ground state of orthorhombic CrN with $\alpha = 88.23°$ has a double-layer antiferromagnetic configuration. However, we are not aware of any experiments which show the magnetic ordering transition for epitaxially stabilized $B1$ structure CrN. In Ref. 13, DFT calculations carried out for $B1$ CrN found the single layer [110]-oriented antiferromagnet to be lower in energy than both the double layer [110], single layer [111], and the ferromagnetic configuration. The single layer [110] ordering in the $B1$ structure is equivalent to the [001] layered antiferromagnet considered in this work.

Four different magnetic configurations were considered. Figure 1 shows the calculated equations of state for the four different configurations of pure CrN, corresponding to a [001]-oriented antiferromagnetic structure, a disordered local moment configuration, and a ferromagnetic and a nonmagnetic configuration. Since the main subject of this work is to describe the properties of $Cr_{1-x}Al_xN$ at elevated temperatures above the Néel temperature, the electronic structure in those cases must be calculated for a disordered magnetic structure. It is known that the DLM model, rather than an ordered magnetic configuration, should be used to accurately calculate thermodynamic properties of magnetic materials with finite local moments above the ordering temperature.[31,32] It was suggested that CrN has localized moments on the Cr sites.[13] It will be apparent from this work that the magnetic degree of freedom, also above the ordering temperature, is crucial to understand the thermodynamics of chemical mixing in $Cr_{1-x}Al_xN$. The DLM approximation uses the CPA to model a system with randomly oriented local magnetic moments. Thus it is a model which allows one to simulate the alloy energetics in the paramagnetic state.

Figure 1 shows that the antiferromagnetic configuration is the lowest in energy among those considered in this work. This result is in agreement with previous calculations on the CrN system.[13] The calculated lattice parameter is 4.196 Å, in good agreement with the experimental one 4.162 Å.[11] Lattice parameters will be discussed in detail in the next
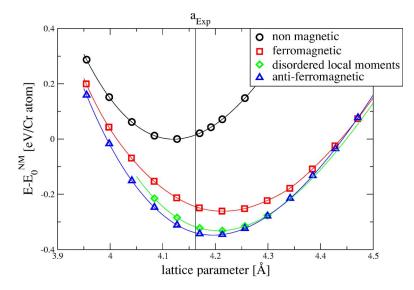
FIG. 1. (Color online) Equation of states for four different magnetic configurations of $B1$ CrN. A [001]-stacked antiferromagnetic configuration (triangles), a configuration with disordered local moments (diamonds), a ferromagnetic configuration (squares), and a nonmagnetic solution (circles) are shown. Energies are given relative to the minimum energy for the nonmagnetic solution E_0^{NM}. The experimental lattice parameter[11] is shown by a vertical line.

section. While the ferromagnetic and the nonmagnetic configurations are considerably above the antiferromagnetic configuration in energy, the DLM solution is only 15 meV per Cr atom higher than the latter. This indicates a stability of the local magnetic moments at the Cr sites while the ordering between them is rather weak. The local moments at Cr sites are $2.20\mu_B$, $2.32\mu_B$, and $2.19\mu_B$ in the antiferromagnetic, DLM, and ferromagnetic cases, respectively.

Figure 2 shows the magnetization energy as a function of AlN content. The figure shows the difference in energy between the three different magnetic configurations and the nonmagnetic solution expressed in electron-volts (eV) per Cr atom. The inset shows a magnification of the energy difference between the [001] ordered antiferromagnetic configuration and the DLM solution (in eV per Cr atom). Since cubic AlN is a nonmagnetic semiconductor the energy differences per formula unit goes to zero as x in $Cr_{1-x}Al_xN$ approaches 1, i.e., when the Cr atoms are more and more diluted. However, to understand thermodynamic properties, such as mixing enthalpy or magnetic ordering energies, it is important to consider magnetization energies per Cr atom as is shown in the main plot of Fig. 2. One can see that the driving force for

magnetization of the Cr atoms increases with increasing Al content. At the same time, as can be seen in the inset, the difference between the antiferromagnetic and the DLM configuration decreases. At the AlN concentration of 20% the DLM solution becomes lower in energy than the [001]-oriented antiferromagnetic configuration. This indicates that there should exist another antiferromagnetic configuration that becomes the ground state at higher AlN content. However, in systems with chemical disorder such as $Cr_{1-x}Al_xN$ one can expect strong effects of the local environment on the orientation of the local magnetic moments.[33,34] A complete ground-state search for the low-temperature magnetic order in $Cr_{1-x}Al_xN$ is beyond the subject of this work since it is focused on high temperature applications. In the Cr-poor regime, where the Cr atoms are quite far away from each other, the different magnetic configurations, including the ferromagnetic one, approach each other in terms of magnetization energy per Cr atom. At the same time the magnitude of the magnetization energy increases rapidly. It is obvious that the system, regardless of AlN content (except the end point $x=1$) needs to be treated within a framework that allows for the spin polarization of the Cr atoms. From this point for-
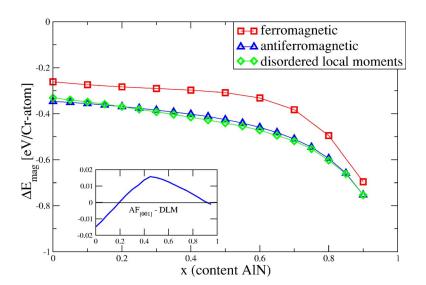

FIG. 2. (Color online) The magnetization energy $E-E_0^{NM}$ per Cr atom (in eV per Cr atom) as a function of AlN content in $Cr_{1-x}Al_xN$. As the content of AlN increases, the magnitude of the magnetization energy of the Cr atoms increases which underlines the importance of a magnetic treatment also in the Cr-poor regime. Inset: The total energy difference per Cr atom between the antiferromagnetic [001] ordered state and the disordered local moment solution (in eV per Cr atom).
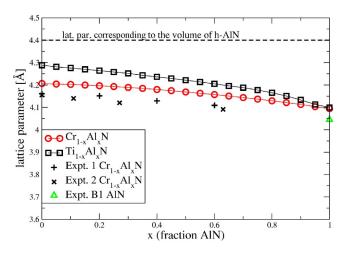
FIG. 3. (Color online) The calculated lattice parameters of $B1$ $Cr_{1-x}Al_xN$ (circles) and $Ti_{1-x}Al_xN$ (squares). For the $Cr_{1-x}Al_xN$ the lattice parameters correspond to the DLM state. Also experimental values for the lattice parameter of $Cr_{1-x}Al_xN$ are shown. Expt. 1 was carried out on cemented carbide substrate[35] and expt. 2 on Si_2O substrate.[12] The experimental value for pure $B1$ AlN (Ref. 36) is shown by a triangle. Also shown is the lattice parameter corresponding to the volume of h-AlN.
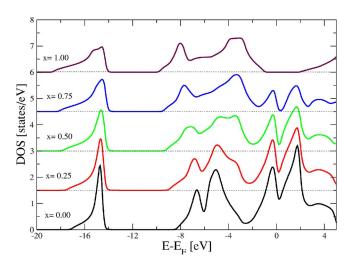

FIG. 4. (Color online) The total density of states for five different compositions of $Cr_{1-x}Al_xN$ calculated within the disordered local moments model. Since the net magnetization vanishes within the DLM, the total DOS is shown. For clarity the curves, $x=0.25$, 0.50, 0.75, and 1.00, are shifted up by 1.5, 3.0, 4.5, and 6.0 states/eV, respectively.

ward, the results of the calculations carried out for the DLM model are reported except when otherwise is explicitly specified.

B. Lattice parameter

Figure 3 shows the calculated lattice parameter of DLM $B1$ $Cr_{1-x}Al_xN$ and (nonmagnetic) $Ti_{1-x}Al_xN$ together with two experimental results for $Cr_{1-x}Al_xN$ (Refs. 12 and 35) as a function of the AlN fraction. The experimental value of high-pressure synthesized $B1$ AlN (Ref. 36) and the lattice parameter corresponding to the calculated volume of wurtzite AlN are shown for comparison.

The calculated lattice parameter of pure CrN in the DLM state is 4.206 Å, very close to the antiferromagnetic lattice parameter of 4.196 Å. This in turn is in very good agreement with the low-temperature experimental value 4.162 Å.[11] The slight overestimation of the lattice constant by 0.8% is typical when using the GGA functional.

The lattice parameter of $Cr_{1-x}Al_xN$ decreases monotonously with increasing AlN content, showing a slight positive deviation from Vegards law. The difference in equilibrium lattice parameter of $B1$ CrN (exp: 4.162 Å,[11] calc: 4.206 Å) and $B1$ AlN (exp: 4.045 Å,[36] calc: 4.094 Å) is very small, less than 3%.

Comparing the system $Cr_{1-x}Al_xN$ with the similar system $Ti_{1-x}Al_xN$ (squares in Fig. 1)[2] indicates that the lattice volume mismatch between end point compounds is even smaller in the Cr-containing alloy. The volume barrier for nucleating the hexagonal $B4$-structure AlN is also larger in this case. The local relaxation energies in the $Cr_{1-x}Al_xN$, system are considerably smaller than in the similar system $Ti_{1-x}Al_xN$ reflecting the smaller difference in equilibrium metal-nitrogen bond length between the components. In DLM $Cr_{0.50}Al_{0.50}N$ the local relaxation energy is 0.011 eV/atom compared to 0.050 eV/atom in $Ti_{0.50}Al_{0.50}N$.[2]

The small lattice mismatch could indicate a low value of the mixing enthalpy. However as was shown in the case of

$Ti_{1-x}Al_xN$ (Ref. 2) the electronic structure factor might be responsible for large mixing enthalpies also in size-matched systems. This will be explored in the next section.

C. Density of states

Figure 4 shows the $Cr_{1-x}Al_xN$ total density of states (DOS) for the valence band at five different compositions, $x=0.00$, 0.25, 0.50, 0.75, and 1.00, as a function of energy relative to the Fermi level. For clarity the curves of composition $x=0.25$, 0.50, 0.75, and 1.00 are shifted by 1.5, 3.0, 4.5, and 6.0 states/eV, respectively. Total DOS for the spin up and spin down channels are the same since the magnetic moments are randomly distributed up and down with equal probability. It should be noted that even though the spin channels are globally degenerate this does not mean that there is no magnetism in the system, since there is a local magnetic splitting of spin up and down electrons at each Cr atom. The latter effect is shown in Fig. 5.
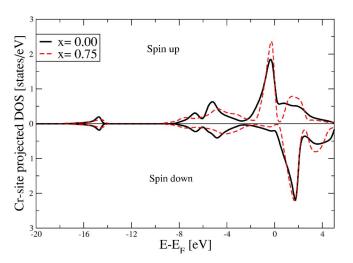

FIG. 5. (Color online) The spin polarized site projected DOS at the Cr site for CrN (solid line) and $Cr_{0.25}Al_{0.75}N$ (dashed line), calculated within the DLM model.

The DOS of pure CrN, i.e., $x=0.00$, is shown as the bottom plot in Fig. 4. The state positioned at about -15 eV is the N $2s$ semicore state that does not participate significantly in the bonding in the system. From about -8 to about -3 eV there is a two-peak bonding state which is formed due to the hybridization between the $3d$ and $2p$ states of nearest neighbor Cr and N atoms, respectively. A pseudogap separates the bonding states from the so called nonbonding states. They consist of Cr $3d$ states with t_{2g} symmetry that, opposite to the $3d$ states with e_g symmetry cannot hybridize strongly with the N $2p$ states. However, they form a weak hybridization with next-nearest neighboring Cr states of the same symmetry. If we do not count the N $2s$ electrons there is nine valence electrons per unit cell in CrN(3N+6Cr). Six electrons can be fitted in the bonding Cr-N states while the remaining three have to be accommodated in the nonbonding Cr states that could hold six electrons in total. If there had been no magnetism in the system, the Fermi level should be located almost at the maximum of the nonbonding peak. This indicates that the Stoner criteria is fulfilled, resulting in a magnetic splitting. One can clearly see this effect in Fig. 5 where the density of states at the Cr site is shown for pure CrN (solid line) and $Cr_{0.25}Al_{0.75}N$ (dashed line). The Cr majority spin (in the local magnetic framework) nonbonding states are almost entirely filled (-2 to 0 eV) and there is only a small overlap with minority spin nonbonding and majority spin antibonding (0–2 eV) states. The hump at about 4 eV corresponds to minority spin antibonding states. The bonding states (-8 to -5 eV) show a negligible magnetic split.

As we pointed out earlier, cubic CrN has been experimentally shown to exhibit a Mott-type insulator behavior at very low temperatures.[11] Such behavior is difficult to reproduce with standard exchange-correlation functionals. However, our calculations of a disordered magnetic state are in very good agreement with the room temperature photoemission measurements.[12]

The obvious effect when Al is added to the system is that the Cr states gradually decrease in intensity. The hybridization between Cr $3d$ and N $2p$ states is gradually reduced and the ionic bonding between Al $3p$ and N $2p$ becomes more dominant. More interestingly the Cr-Cr next-nearest neighbor hybridization is weakened, resulting in a transformation of the nonbonding Cr $3d$ states into atomic-like impurity states which can be seen both in Figs. 4 and 5.

However, in contrast to the system $Ti_{1-x}Al_xN$, where the formation of such a sharp state leads to a drastic increase of the Ti site-projected DOS at the Fermi level,[2] the opposite effect happens in $Cr_{1-x}Al_xN$. The magnetic splitting of the nonbonding state leads to a situation where the nonbonding spin up state becomes more and more occupied approaching the maximum of three electrons while the spin down counterpart is pushed above the Fermi level. Thus the Fermi level is shifted down the slope of the majority spin state as Cr-Cr hybridization decreases and with high enough Al content the system shows semiconducting behavior. In the $Ti_{1-x}Al_xN$-case the system stays nonmagnetic over the whole concentration range, possibly with the exception of a minimal splitting in the extreme case of a single Ti impurity in semiconducting AlN. This is so since in $Ti_{1-x}Al_xN$ there is only one electron per Ti atom that needs to be accommodated by the nonbonding states. Regardless if this state is magnetically split or not, the Fermi level falls onto the peak, minimizing the energy which could be gained due to magnetization. Pure $B1$ AlN is predicted to be a semiconductor with a band gap of about 3 eV. Both concentration dependent trends and the relative intensity of different peaks of the calculated DOS of $Cr_{1-x}Al_xN$ show good agreement with the x-ray photoelectron spectroscopy experiments in Ref. 12.

In summary, the electronic structure effects, that destabilize AlN rich $Ti_{1-x}Al_xN$ is absent in the case of $Cr_{1-x}Al_xN$. The consequences for the mixing enthalpies in the two systems will be apparent in the next section.

D. Mixing enthalpy

The isostructural mixing enthalpy

$$H(x) = E(Cr_{1-x}Al_xN) - (1-x)E(CrN) - xE(c-AlN) \quad (1)$$

has been calculated for $Cr_{1-x}Al_xN$ with concentration steps of $x=0.05$. The energies are taken for the calculated equilibrium volume for each specific concentration, thus setting the pressure-volume term of the enthalpies to zero. This gives a total of 21 points on the mixing enthalpy curve. The magnetic state relevant for thin film growth and applications at elevated temperatures is the DLM state as has been shown in Sec. III A. It has been shown[32] that the mixing enthalpies calculated for the ordered and disordered magnetic states can differ qualitatively. However, also a nonmagnetic calculation gives qualitatively different results compared to the DLM description of the paramagnetic phase of $Cr_{1-x}Al_xN$ as can be seen in Fig. 6. The figure shows the mixing enthalpy calculated for the DLM state and the nonmagnetic state of $Cr_{1-x}Al_xN$ in eV per atom as a function of AlN content. The mixing enthalpy calculated for the DLM state is very symmetric with respect to equiatomic composition with its maximum 0.037 eV/atom at about $x=0.50$. On the other hand, the mixing enthalpy of the nonmagnetic system shows a nonsymmetric curve shifted to the AlN-rich side and with a maximum of 0.065 eV per atom. The difference underlines that only a model that allows for disordered magnetism, like the DLM, could be used to accurately calculate the thermodynamic properties of $Cr_{1-x}Al_xN$ at relevant temperatures. The inset in Fig. 6 shows the mixing enthalpy relative to the wurtzite ground state structure of AlN. The structural energy difference between $B1$ (cubic rock-salt) and $B4$ (hexagonal wurtzite) AlN is 0.178 eV/atom. This indicates that at almost all temperatures and fractions of AlN, the cubic mixture can at the most be metastable, which, however, is sufficient for the successful use of $Cr_{1-x}Al_xN$ in hard coatings applications.

Figure 7 shows a comparison between the mixing enthalpies of $Cr_{1-x}Al_xN$ (bold dashed line) and $Ti_{1-x}Al_xN$ (bold solid line) as well as their second concentration derivatives ($Cr_{1-x}Al_xN$: thin dashed line, $Ti_{1-x}Al_xN$: thin solid line). As seen in Fig. 7 there are both striking qualitative and quantitative differences between the mixing enthalpies of the $Cr_{1-x}Al_xN$ and the $Ti_{1-x}Al_xN$ systems. First, the mixing enthalpy of $Ti_{1-x}Al_xN$ is about two to three times larger than
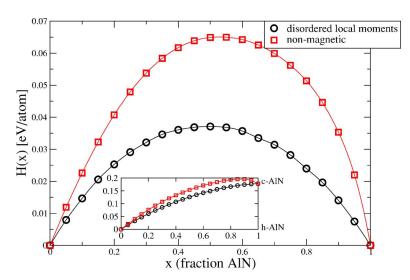
FIG. 6. (Color online) Isostructural mixing enthalpy $H(x)$ of $B1$ $Cr_{1-x}Al_xN$. Shown are the results of non-magnetic (squares) and magnetic (circles) treatment within the disordered local moments model. The huge difference underlines the importance of including the magnetic effects also when modeling systems above the Néel temperature. Inset: The mixing enthalpy relative to the stable wurtzite structure of AlN.

that of $Cr_{1-x}Al_xN$ for all concentrations except for the regime with very low fraction of AlN. Second, the shape of the $Ti_{1-x}Al_xN$ enthalpy curve is highly asymmetric in contrast to $Cr_{1-x}Al_xN$ which shows a very symmetric behavior with respect to equal fractions of CrN and AlN. This difference becomes more striking when considering the second concentration derivative. While the second derivative of the $Cr_{1-x}Al_xN$ curve shows a smooth parabola, the second derivative of $Ti_{1-x}Al_xN$ curve goes to very large negative numbers as the content of AlN increases above $x=0.50$. The latter is a direct result of the electronic structure variations with alloy composition, as described earlier and in Ref. 2. Indeed an atomic-like Ti d state is formed at the Fermi level at high AlN content while there is no such counterpart in the Cr case due to the magnetic splitting. Since the second concentration derivative of the free energy is directly related to the tendency for a mixture to decompose through the spontaneous
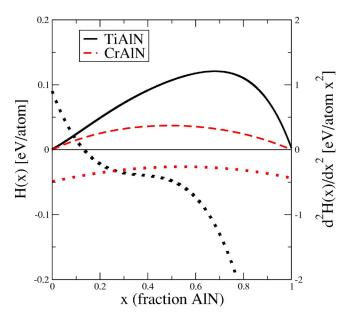
spinodal mechanism, the results shown in Fig. 7 can be used to predict the hypothetical 0 K limit of regions of metastability and instability in the systems. More importantly, it is the starting point for finite temperature predictions.

A first approximation for the entropy contribution to the alloy free energy is the mean field approximation used to derive the phase diagram in Ref. 2. This approximation predicts that $Ti_{1-x}Al_xN$, if diffusion barriers are overcome, is subject to spinodal decomposition over almost the entire composition range at temperatures relevant for hard coatings applications. At 1000 °C the spinodal region of $Ti_{1-x}Al_xN$ is predicted to be from $x=0.25$ to $x=0.99$.[2] If the same approximation is applied to the $Cr_{1-x}Al_xN$ system the spinodal region at 1000 °C would be from $x=0.23$ to $x=0.70$. However, those numbers should be taken as an upper limit of the extent of the spinodal region since the mean field approximation is known to generally overestimate transition temperatures and that vibrational entropy and strain effects are not considered. In any case, coatings with medium or high AlN content, which have large potential for industrial applications, are predicted to show much weaker tendency toward decomposition in $Cr_{1-x}Al_xN$ compared to $Ti_{1-x}Al_xN$. The unusual effect in $Ti_{1-x}Al_xN$, that the end point of the isostructural decomposition are samples with regions of almost pure c-AlN, is absent in the case of $Cr_{1-x}Al_xN$. If spinodal decomposition do occur in the latter system it should end with regions of Cr- or Al-enriched $Cr_{1-x}Al_xN$. Since the composition difference between such domains would be smaller and since the concentration dependence of the lattice parameter is rather week, see Fig. 3, the strain fields induced by isostructural decomposition in $Cr_{1-x}Al_xN$ are expected to be much weaker than in the $Ti_{1-x}Al_xN$ system. Since such strains are thought to be the reason for the age hardening in the Ti-containing system[1] we expect no, or a minimal, age hardening effect for the $B1$ structure of $Cr_{1-x}Al_xN$. On the other hand, at even higher temperatures where the strained domains of $Ti_{1-x}Al_xN$ are relaxed by the introduction of dislocations the loss of coherency leads to a drastic loss in hardness. In $Cr_{1-x}Al_xN$ coherency in the material should be able to survive higher temperatures.

Experimentally the thermal stability of the $Cr_{1-x}Al_xN$ has been explored in Refs. 8 and 37. It was found that the

FIG. 7. (Color online) Comparison between isostructural mixing enthalpies $H(x)$ (left hand axis) of $B1$ $Cr_{1-x}Al_xN$ (bold dashed line) and $Ti_{1-x}Al_xN$ (bold solid line) and between their second concentration derivatives d^2H/dx^2 (right hand axis), $Cr_{1-x}Al_xN$ (thin dashed line), and $Ti_{1-x}Al_xN$ (thin solid line). Note the qualitative difference of the behavior of the second derivatives calculated for the two systems.

single phase cubic $B1$ structure is obtained for samples with $x \leq 0.71$. Pure CrN starts to lose nitrogen already at 750 °C but this process is shifted to higher temperatures, between 900 and 1000 °C, with AlN fraction of 0.46 and 0.71. Above the nitrogen release temperature a series of phase transformations take place, resulting in the formation of Cr_2N, body-centered-cubic Cr and hexagonal-close-packed Al(Cr)N. Below the nitrogen release temperature the $B1$ cubic phase is totally dominating, but in the coating with $x = 0.71$ small amounts of hexagonal AlN nucleate already at temperatures below 800 °C.

For the matter of comparison with the present study, the x-ray diffraction evidence of spinodal decomposition, within the cubic phase present in the $Ti_{1-x}Al_xN$ system at temperatures between 600 and 950 °C,[1,3] is absent in the case of $Cr_{1-x}Al_xN$. Also the age hardening effect seen at temperatures between 600 and 950 °C in the $Ti_{1-x}Al_xN$ films is not seen in the $B1$ structured Cr-based coatings.[8,37]

IV. CONCLUSIONS

In conclusion we have performed first-principles calculations of the magnetic structure, lattice parameter, electronic structure, and mixing enthalpy for the cubic $B1$ structure of $Cr_{1-x}Al_xN$. The results are compared with those for the similar system $Ti_{1-x}Al_xN$ and with experiments.

We have considered four magnetically different configurations and found that for pure CrN the energies of a [001]-ordered antiferromagnetic spin structure and a disordered local moments configuration are very close. The difference is only 0.015 eV/Cr atom at their respective equilibrium lattice parameters. On the other hand, the magnetization energy, which we calculate as the difference between the antiferromagnetic and nonmagnetic solutions, is much larger, 0.347 eV/Cr atom. The energy of the ferromagnetic configuration falls in between the antiferromagnetic and the nonmagnetic ones. The magnetization energy per Cr atom increases with increasing fraction of AlN. These results indicate that the use of the disordered local moments approximation rather than nonmagnetic calculations is important to model the $Cr_{1-x}Al_xN$ system at elevated temperatures.

The calculated lattice parameters are in good agreement with the experimental values. The difference between CrN and $B1$ AlN is small, less than 3%, indicating a small lattice mismatch contribution to the isostructural mixing enthalpy.

The density of states is calculated for the disordered local moment model and shows a clear impact of magnetic splitting. The Cr $3d$ nonbonding state is magnetically split, so the Fermi level is located in a valley between two peaks. This effect is accentuated with increasing AlN content leading eventually to a semiconducting behavior. Thus the effect reported in Ref. 2, where the Ti site projected DOS at the Fermi level increases with AlN content, does not occur in the case of $Cr_{1-x}Al_xN$.

The isostructural mixing enthalpy of $Cr_{1-x}Al_xN$ is drastically lower than the enthalpy of $Ti_{1-x}Al_xN$. Their second concentration derivatives also show qualitatively different shape due to the difference in the electronic structure induced by the magnetic splitting of the nonbonding Cr $3d$ states in $Cr_{1-x}Al_xN$. To a minor part the even smaller size mismatch between $B1$ structure CrN and AlN, compared to TiN and AlN, contributes to a lower enthalpy.

The results show that the tendency toward isostructural spinodal decomposition is much weaker in the Cr-containing system compared to the Ti-based one. This explains the possibility to create metastable cubic $Cr_{1-x}Al_xN$ with higher amount of AlN compared to $Ti_{1-x}Al_xN$ and the absence of an age hardening effect in $Cr_{1-x}Al_xN$ below 900 °C. The latter is present in $Ti_{1-x}Al_xN$. The lower tendency toward decomposition at intermediate temperatures keeps the lattice of $Cr_{1-x}Al_xN$ more stable and coherent, resulting in a retained hardness at even higher temperatures.

[1] P. H. Mayrhofer, A. Hörling, L. Karlsson, J. Sjölén, T. Larsson, C. Mitterer, and L. Hultman, Appl. Phys. Lett. **83**, 2049 (2003).
[2] B. Alling, A. V. Ruban, A. Karimi, O. E. Peil, S. I. Simak, L. Hultman, and I. A. Abrikosov, Phys. Rev. B **75**, 045123 (2007).
[3] A. Hörling, L. Hultman, M. O. J. Sjölén, and L. Karlsson, Surf. Coat. Technol. **191**, 384 (2005).
[4] X. Z. Ding and X. T. Zeng, Surf. Coat. Technol. **200**, 1372 (2005).
[5] R. Wuhrer and W. Yeung, Scr. Mater. **50**, 1461 (2004).
[6] H. Hasegawa and T. Suzuki, Surf. Coat. Technol. **188–189**, 234 (2004).
[7] A. Horling, L. Hultman, M. Oden, J. Sjölen, and L. Karlsson, J. Vac. Sci. Technol. A **20**, 1815 (2002).
[8] A. E. Reiter, V. H. Derflinger, B. Hanselmann, T. Bachmann, and B. Sartory, Surf. Coat. Technol. **200**, 2114 (2005).
[9] L. M. Corliss, N. Elliott, and J. M. Hastings, Phys. Rev. **117**, 929 (1960).
[10] R. M. Ibberson and R. Cywinski, Physica B (Amsterdam) **180–181**, 329 (1992).
[11] D. Gall, C. S. Shin, R. T. H. I. Petrov, and J. E. Greene, J. Appl. Phys. **91**, 5882 (2002).
[12] R. Sanjinés, O. Banakh, C. Rojas, P. E. Schmid, and F. Lévy, Thin Solid Films **420–421**, 312 (2002).
[13] A. Filippetti, W. E. Pickett, and B. M. Klein, Phys. Rev. B **59**, 7043 (1999).
[14] H. Hugosson, H. Högberg, M. Algren, M. Rodmar, and T. I. Selinder, J. Appl. Phys. **93**, 4505 (2003).
[15] T. Suzuki, Y. Makino, M. Samandi, and S. Miyake, J. Mater. Sci. **35**, 4193 (2000).
[16] H. L. Skriver and N. M. Rosengaard, Phys. Rev. B **43**, 9538 (1991).
[17] I. A. Abrikosov and H. L. Skriver, Phys. Rev. B **47**, 16532 (1993).
[18] A. V. Ruban and H. L. Skriver, Comput. Mater. Sci. **15**, 119 (1999).
[19] J. Korringa, Physica **13**, 392 (1947).
[20] W. Kohn and N. Rostocker, Phys. Rev. **94**, 1111 (1954).
[21] O. K. Andersen, Phys. Rev. B **12**, 3060 (1975).
[22] O. K. Andersen and O. Jepsen, Phys. Rev. Lett. **53**, 2571 (1984).
[23] P. Soven, Phys. Rev. **156**, 809 (1967).
[24] B. Velický, S. Kirkpatrick, and H. Ehrenreich, Phys. Rev. **175**, 747 (1968).
[25] S. Kirkpatrick, B. Velický, and H. Ehrenreich, Phys. Rev. B **1**, 3250 (1970).
[26] B. L. Gyorffy, A. J. Pindor, J. Staunton, G. M. Stocks, and H. Winter, J. Phys. F: Met. Phys. **15**, 1337 (1985).
[27] J. Perdew, K. Burke, and M. Ernzerhof, Phys. Rev. Lett. **77**, 3865 (1996).
[28] P. E. Blöchl, Phys. Rev. B **50**, 17953 (1994).
[29] G. Kresse and J. Hafner, Phys. Rev. B **48**, 13115 (1993).
[30] G. Kresse and J. Hafner, Phys. Rev. B **49**, 14251 (1994).
[31] A. E. Kissavos, S. I. Simak, P. Olsson, L. Vitos, and I. A. Abrikosov, Comput. Mater. Sci. **35**, 1 (2006).

[32]P. Olsson, I. A. Abrikosov, L. Vitos, and J. Wallenius, J. Nucl. Mater. **321**, 84 (2003).

[33]A. V. Ruban, M. I. Katsnelson, W. Olovsson, S. I. Simak, and I. A. Abrikosov, Phys. Rev. B **71**, 054402 (2005).

[34]I. A. Abrikosov, F. Liot, T. Marten, and E. A. Smirnova, J. Magn. Magn. Mater. **300**, 211 (2006).

[35]A. Kimura, M. Kawate, H. Hasegawa, and T. Suzuki, Surf. Coat. Technol. **169–170**, 367 (2003).

[36]H. Vollstädt, E. Ito, M. Akaishi, S. Akimoto, and O. Fukunaga, Proc. Jpn. Acad., Ser. B, Phys. Biol. Sci. **66**, 7 (1990).

[37]H. Willmann, P. H. Mayrhofer, P. Persson, A. E. Reiter, L. Hultman, and C. Mitterer, Scr. Mater. **54**, 1847 (2006).